ACCSCIENCE PUBLISHING

International Journal of Bioprinting

REVIEW ARTICLE

AI-driven integration of multimodal CT/MRI imaging and 3D printing in medicine: Advances, clinical applications, and future directions

Weipeng Zhou, Lihua Gao, Meng Wu, and Jianhua Liu*

Department of Radiology, The Second Hospital of Jilin University, Changchun, Jilin, China

(This article belongs to the *Special Issue*: *3D-Printed Biomedical Devices*)

Abstract

The integration of artificial intelligence (AI)-enabled multimodal computed tomography (CT)/magnetic resonance imaging (MRI) medical imaging and three-dimensional (3D) printing technology represents a pivotal direction in medical engineering for advancing precision diagnosis and therapy. Multimodal data fusion serves as the primary strategy to enhance the accuracy of 3D-printed models; however, cross-modal data fusion is hindered by inherent technical challenges, including failures in feature alignment and discrepancies in the physical properties of imaging datasets. In recent years, the advancement and seamless integration of AI technology have emerged as the core link bridging the entire workflow, from multimodal CT/MRI imaging acquisition to 3D printing, offering novel paradigms for the development of high-precision 3D printing technology in clinical settings. This review systematically elaborates on AI's core technical underpinnings for multimodal imaging and 3D printing: AI effectively mitigates integration and adaptation hurdles arising from intrinsic discrepancies in data source characteristics through three key pathways—artifact reduction and optimization of raw imaging data, precise cross-modal registration, and fine-grained segmentation of anatomical structures. Furthermore, AI-driven optimization of 3D rendering effects, combined with four-view projection, significantly enhances the fidelity of anatomical detail reproduction, thereby minimizing the matching error between 3D-printed models and *in vivo* physical entities. Subsequently, the review details the clinical application value of multimodal 3D printing technology across key medical specialties, including orthopedics, oncological surgery, dentistry, and vascular surgery, while concomitantly highlighting prevailing challenges in technical translation and clinical adoption. Finally, it outlines future development directions from three critical dimensions: technological synergy (among AI, imaging, and 3D printing), material advancement (targeting durability and functional adaptability), and application expansion (to underserved clinical scenarios such as rehabilitation). This work aims to provide a comprehensive reference for accelerating the clinical translation of this interdisciplinary technology.

Keywords: 3D printing technology; AI-enabled image preprocessing; Cross-modal data alignment; Multimodal CT/MRI imaging

***Corresponding author:**
Jianhua Liu
(Jian_hua@jlu.edu.cn)

Citation: Zhou W, Gao L, Wu M, Liu J. AI-driven integration of multimodal CT/MRI imaging and 3D printing in medicine: Advances, clinical applications, and future directions *Int J Bioprint*. 2026;12(1):125-144. doi: 10.36922/IJB025390404

Received: September 28, 2025
Revised: November 2, 2025
Accepted: November 3, 2025
Published online: November 7, 2025

1. Introduction

In the current era of precision medicine's deep evolution toward "personalized diagnosis and treatment," the convergence of medical imaging technology and advanced manufacturing technology has emerged as a core strategy for addressing complex clinical diagnostic and therapeutic challenges.[1,2] Multimodal computed tomography (CT) and magnetic resonance imaging (MRI) stand as primary modalities for clinical diagnosis and preoperative assessment, each exhibiting distinct technical strengths. CT, with its high spatial resolution and rapid imaging capabilities, enables clear visualization of hard-tissue details (e.g., bone structures, calcifications), providing precise osseous landmarks for anatomical localization. MRI, by contrast, excels in delineating tumor margins, neurovascular trajectories, and the extent of tissue edema due to its superior soft-tissue contrast resolution, addressing the gap in functional and soft-tissue assessment that persists with hard-tissue-dominant imaging.[3–5]

However, both modalities have inherent technical limitations. CT imaging relies on ionizing X-ray radiation, and repeated or high-dose scans increase radiation exposure risks for patients. Additionally, its inherently low soft-tissue contrast constrains the visualization of small lesions and soft-tissue tumors, and it is highly prone to metal-induced artifacts that obscure the observation of adjacent structures.[6,7] While MRI avoids radiation hazards, it suffers from high equipment costs and limited accessibility; further, examination durations are prolonged, rendering it less suitable for patients with intravascular or implanted metallic devices, critically ill individuals, and those unable to maintain prolonged immobilization (e.g., infants, agitated patients). Concurrently, its imaging performance for air-filled organs (e.g., lungs, gastrointestinal tract) and osseous structures remains suboptimal.[8–10]

The isolated application of single-modal CT or MRI images cannot accurately reconstruct the detailed information of various anatomical structures in the human body.[11] Moreover, their simple superposition leads to issues such as data misalignment and artifact interference due to differences in their imaging principles, which restrict the fidelity of digital models. Therefore, the precise fusion of multimodal CT/MRI imaging data constitutes a critical bottleneck in achieving the transformation from "virtual images to physical models" during the interdisciplinary integration of medical imaging technology and advanced manufacturing technology.

Three-dimensional (3D) printing technology is one of the most rapidly advancing manufacturing methods in recent years and is categorized under rapid prototyping. Medical imaging-based 3D printing begins with acquiring raw anatomical data using medical imaging scanners, followed by generating 3D-printable stereolithography (STL)-format models through sequential steps: 3D reconstruction, model segmentation, and optimization. Controlled by the 3D printing system, filamentous, liquid, or powdered feedstocks are deposited and layered with precise spatial positioning, ultimately producing physical anatomical models that closely replicate *in vivo* structures.[12]

The selection of 3D printing technologies in medical applications must primarily balance precision, cost, and biocompatibility. Each mainstream technology possesses unique adaptive characteristics. SLA/digital light processing achieves a precision of 20–50 μm, is compatible with biocompatible photosensitive resins, and is suitable for scenarios requiring high precision, such as dental implant guides. Binder jetting (BJ) utilizes titanium alloy and hydroxyapatite as raw materials, offers excellent biocompatibility, and is well-suited for orthopedic implant manufacturing. Material extrusion (fused deposition modeling [FDM]) is cost-effective, can print materials such as poly(lactic acid), and is mostly used for educational phantoms. Bioprinting specifically refers to the precise deposition of living cells, biomaterials (e.g., hydrogels), and bioactive molecules through layer-by-layer deposition to construct functional biological structures such as tissues, organs, or organoids. Matching the performance requirements of different technologies provides key guidance for clinical selection.[13]

The advent and advancement of 3D printing have established a critical technical platform for translating medical imaging data into physical constructs. Medical imaging-based 3D printing transforms digital imaging data into scaled, clinically actionable physical anatomical models, providing tangible tools for preoperative planning (e.g., tumor resection simulation), surgical rehearsal, and personalized implant design.[14] The accuracy and clinical applicability of 3D printing essentially depend on the quality of the digital model generated from upstream imaging data. If the precise fusion and optimization of CT/MRI multimodal images are not achieved, 3D printed models will struggle to balance the anatomical fidelity of hard and soft tissues, thereby losing their clinical guiding value. Therefore, constructing multimodal imaging data into a digital model with high accuracy and compatibility with 3D printing processes is the core challenge in achieving clinical translation.

The concept of artificial intelligence (AI) first emerged several decades ago. However, recent breakthrough advancements in machine learning (ML) and neural

network (NN)-based algorithms have sparked a profound revolution in the field.[15] The integration of AI with 3D printing, particularly when combined with multimodal imaging, has become a prominent research focus in recent years. The historical stages and progress of this integration are summarized in Table 1.

Against this backdrop, the integration of AI technology has become the core link connecting the entire workflow of "multimodal CT/MRI imaging–3D printing".[16] In recent years, AI-assisted multimodal CT/MRI–3D printing interdisciplinary technology has been applied in fields such as orthopedics, oncological surgery, dentistry, and vascular surgery.[17–19] However, current research still faces numerous issues that hinder the technology's transition from the "laboratory" to "clinical application." Therefore, this paper aims to systematically summarize the research progress and clinical practice outcomes of the interdisciplinary application of multimodal CT/MRI imaging and 3D printing technology, analyze the current technical and clinical challenges, and propose future breakthrough directions. It provides a reference for promoting the development of this interdisciplinary field toward "high fidelity, high adaptability, and standardization," and facilitates the in-depth integration of precision medicine with the diagnosis and treatment of complex diseases.

2. Core technology support for multimodal CT/MRI and 3D printing

Within the integrative framework of multimodal CT/MRI and 3D printing technologies, AI assumes a central role, with its technical interventions encompassing the entire workflow of their integration. On one hand, by addressing the inherent data heterogeneity of multimodal imaging, AI mitigates compatibility challenges across different modalities. Through a sequence of operations—including preprocessing optimization (e.g., denoising, contrast enhancement), high-precision cross-modal registration, and fine-grained anatomical segmentation—AI converts raw imaging data into high-fidelity anatomical digital templates that meet the stringent requirements of 3D printing. On the other hand, AI facilitates the critical interface stage between multimodal imaging and 3D printing: it enhances the reproduction fidelity of micro-anatomical details via advanced 3D rendering techniques while providing data-driven guidance for subsequent adjustments of 3D printing parameters (e.g., layer height, infill density). This dual functionality minimizes precision discrepancies caused by workflow fragmentation between technical stages. Figure 1 illustrates the complete technical roadmap for the integration of AI-driven multimodal CT/MRI and 3D printing.

2.1. Artificial intelligence-assisted preprocessing techniques for multimodal imaging

Multimodal imaging, by integrating imaging data from diverse modalities (e.g., CT and MRI), underpins the establishment of digital models with more holistic information. However, during data acquisition, multimodal imaging data are prone to degradation caused by factors such as variations in equipment parameters, patient positional shifts, tissue motion artifacts, and noise interference. Such perturbations contribute to spatial misregistration, inhomogeneous gray-level intensity, and disparate feature scales across different modalities—severely compromising the accuracy of digital model construction.[20–22] As a

Table 1. Development history of artificial intelligence (AI) in medical image segmentation and 3D printing

Development stage	Core AI technology type	Representative algorithm/model	3D printing applicable scenario	Key progress
Early exploration stage (2010–2015)	Traditional machine learning	Support vector machine, random forest	Simple osseous structures (e.g., femur, skull)	Enabled semi-automatic segmentation of medical images; model error exceeded 1 mm, and was applicable only to non-weight-bearing bone models
Rapid development stage (2016–2020)	Basic deep learning	U-Net, ResNet, FCN	Soft tissue tumors (e.g., liver cancer), large blood vessels	Achieved breakthroughs in end-to-end segmentation; Dice coefficient increased to 0.85–0.90, and model error was reduced to 0.5–1.0 mm
Precision optimization stage (2021–present)	Optimized deep learning	ECR-UNet, dual U-Net, CTGANs, Res-UNet	Calcified tumors, small blood vessels, repair of bone defects	Introduced attention mechanism and cross-modal fusion; Dice coefficient exceeded 0.91, supporting naked-eye 3D visualization and personalized implant printing with an error of less than 0.5 mm

Abbreviations: CTGANs, conditional tabular generative adversarial networks; ECR, express connect router; FCN, fully convolutional network; Res, residual.

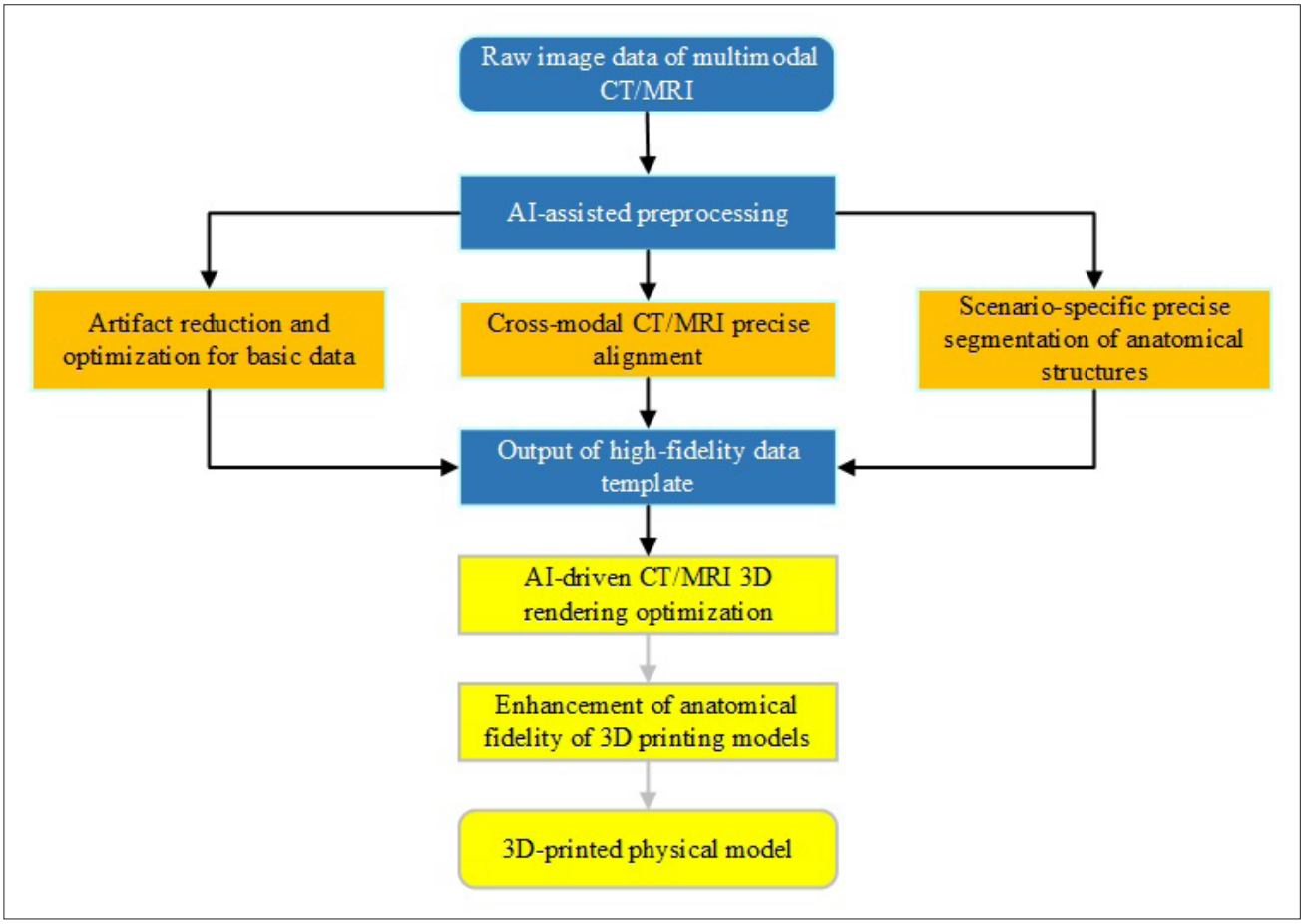

Figure 1. Artificial intelligence-driven flowchart of multimodal computed tomography (CT)/magnetic resonance imaging (MRI)–3D printing fusion.

pivotal component of the multimodal imaging analysis workflow, the core objective of preprocessing is to refine data quality through procedures such as noise reduction, normalization, spatial registration, modality alignment, and weak data adaptation.[20] Traditional preprocessing methods rely on manual expertise for parameter tuning, leading to cumbersome workflows, low efficiency, and poor generalizability—limitations that render them inadequate for processing large-scale multimodal imaging datasets. In contrast, AI technology models the inherent correlations and feature patterns of multimodal data via deep learning and related algorithms. It enables intelligent processing capabilities, including adaptive noise suppression, precise cross-modal spatial registration, and dynamic gray-level normalization, thereby substantially enhancing the efficiency, accuracy, and robustness of preprocessing.[23] Consequently, it delivers high-quality data support for subsequent 3D printing.

2.1.1. Classification of machine learning models and data foundations for multimodal fusion

In multimodal imaging preprocessing workflows, ML models are categorized into the following three groups based on their alignment with clinical demand scenarios.

(a) Supervised learning models for multimodal fusion

One of the primary objectives of multimodal imaging preprocessing is to achieve precise alignment of CT and MRI data, as well as accurate segmentation of anatomical structures (e.g., tumor boundary extraction, bone structure localization). Using annotated data such as segmentation masks and alignment labels, these models learn the mapping between inputs (raw imaging data) and outputs (segmentation and alignment results), thereby fulfilling the requirements for precise segmentation and alignment.

In terms of performance, these models demonstrate significant accuracy advantages. For instance, the dual U-Net network achieves a Dice similarity coefficient of

0.864 for cross-modal alignment,[24] while the ECA CBAM Res (ECR)–U-Net attains an 89.13% Dice similarity coefficient for segmenting tumor calcification regions.[25] Additionally, they can visualize key regions, such as tumor boundaries, through feature maps. However, certain limitations must be acknowledged: these models require large-scale annotated datasets (e.g., the training of ECR-UNet relies on 153 whole-slide pathological sections from 39 tumor patients[25]), and varying quality of labeled data may affect model performance. To mitigate the impact of device variability, targeted optimization of data quality during training is essential. For example, improved 3D deep convolutional neural network (iDCNN) processes brain MRI data from 46 patients with Wilson's disease (WD) using "four-fold rotation and grayscale normalization",[26] whereas dual U-Net addresses device bias in CT/MRI data from 12 patients undergoing anterior cruciate ligament (ACL) reconstruction through " deformation field and the non-rigid registration fusion module".[24]

These models directly provide high-fidelity multimodal fused data for clinical scenarios such as tumor preoperative planning and orthopedic implant design. Even when constrained by factors such as limited data scale and device variability, these models can still satisfy the multimodal integration requirements of most routine cases through optimization techniques like data normalization, thereby establishing a robust data foundation for subsequent precision medical procedures.

One recent study[27] demonstrates that Residual (Res)–U-Net transfer learning offers significant advantages in cerebrovascular segmentation: it addresses the gradient vanishing problem in deep networks through residual connections, achieving a segmentation Dice coefficient of 0.914. Furthermore, its segmentation results can be directly exported as STL files (without additional format optimization), reducing 3D printing preparation time.

(b) Generative models for small-sample scenarios

In clinical practice, the volume of imaging data for rare diseases (e.g., mandibular tumors) or specific postoperative cases is often insufficient to support model training, necessitating the use of "data generation" to supplement samples. Generative models, such as conditional tabular generative adversarial networks (CTGANs), employ an adversarial training mechanism involving a generator and discriminator to produce anatomically consistent synthetic data based on a limited amount of real data. This approach makes them well-suited for scenarios involving data completion or small-sample augmentation.

The core value of these models lies in overcoming limitations related to data volume. For example, Ref. 28 utilized only 27 cases of postoperative CT data of mandibular tumors to generate virtually complete samples of defect regions, effectively repairing incomplete images such as mandibular defects. During training, "defect region masks" were used as inputs and "completed mandibular models" as outputs. Data quality was evaluated using mean squared error (MSE = 2411.9 ± 833.6) to ensure the anatomical plausibility of the generated data. However, the training process is unstable and prone to "mode collapse" (producing repetitive structures); thus, the generated results must be validated clinically.

Although clinical validation of generated results is necessary, incorporating anatomical rationality evaluations (e.g., the MSE metric) effectively broadens the scope of medical applications for multimodal imaging, enabling more patients with unique cases to benefit from AI-assisted precision diagnosis and treatment.

(c) Object detection models for real-time localization in intraoperative navigation

Intraoperative navigation demands the rapid identification of key anatomical structures, such as lumbar pedicles, and places extremely high requirements on model processing speed. Object detection models, exemplified by You Only Look Once version 5x (YOLOv5x), utilize an "end-to-end detection" mechanism that directly outputs the locations of target regions, making them well-suited for real-time localization scenarios.

The primary advantage of these models is their high processing efficiency (>20 frames per second), which enables real-time intraoperative navigation. However, due to inherent limitations in their detection principles, their accuracy in identifying small targets (e.g., tiny calcifications) remains relatively low.[25,29] During the training phase, maintaining consistency in data annotation is essential. For example, using over 100 cases of lumbar CT data, pedicle centers are annotated, and annotation quality is assessed using the Kappa coefficient to minimize annotation bias and ensure accurate model localization.[30]

From the perspective of clinical translation needs, these models transform preoperative multimodal imaging data (CT/MRI) into intraoperative real-time navigation information, directly supporting precision surgical procedures such as orthopedic pedicle screw implantation. Although their accuracy in detecting small targets is limited, they can still satisfy the clinical requirements for most intraoperative real-time localization tasks through targeted annotation optimization (e.g., precise annotation of pedicle centers).

2.1.2. Basic data optimization

As a foundational component of data optimization, the preprocessing stage poses distinct challenges to

AI in processing multimodal imaging data. These challenges primarily manifest in three core issues: weak signal detection challenges, incomplete lesion region modeling, and interference from modality-specific structural artifacts. Regarding weak signal detection, low-contrast features arising from the intrinsic limitations of imaging modalities (e.g., subtle infiltration signals of early tumors or slight density changes in cerebral white matter rarefaction) impede AI models from capturing their statistical patterns through a single feature channel. Furthermore, rare diseases—characterized by low incidence rates—lack sufficient high-quality annotated MRI samples, compromising the model's capacity to fully acquire disease-specific features.[26] The complexity of lesion region modeling also represents a major bottleneck restricting the precise development of 3D-printed digital models. This stems from the morphological heterogeneity of lesion tissues, their ill-defined boundaries, and disrupted topological associations with normal anatomical structures. For instance, pathological changes such as tissue boundary erosion due to tumor invasion, discrete distribution of bone fragments post-fracture, surgical tissue defects, and infection-induced soft tissue swelling render traditional threshold-based segmentation or morphology-driven modeling approaches incapable of accurately delineating lesion extents. Over-segmentation may erroneously incorporate normal tissues into the lesion area, causing volume distortion in 3D-printed models, while under-segmentation may omit small lesions or critical structures—leading to misjudgments regarding the extent of lesion invasion during surgical planning.[23,31] Interference from modality-specific structural artifacts is even more technically intricate. For example, star-burst artifacts induced by metal implants in CT and chemical shift artifacts resulting from magnetic field inhomogeneity in MRI not only exhibit modality-specific, morphologically diverse features but also frequently induce signal ambiguity with adjacent anatomical structures (e.g., cortical bone surrounding orthopedic implants or gray matter near intracranial metal foreign bodies). This requires AI algorithms to preserve structural fidelity while suppressing artifacts, avoiding the loss of anatomical details caused by over-processing.[32]

To mitigate these challenges, AI technology has employed multi-faceted strategies to achieve targeted breakthroughs. For weak signal detection, it leverages multi-scale feature fusion networks integrated with attention mechanisms to enhance the hierarchical representation of low-contrast features, and it utilizes cross-modal associative learning to explore potential mapping patterns between signals.[33] For deficiencies in lesion region modeling, it incorporates a transfer learning framework to transfer general anatomical knowledge to small-sample scenarios and employs generative adversarial networks to generate anatomically consistent virtual lesion samples for training set expansion.[31,28] For modality-specific artifacts, it develops physics-constrained adversarial denoising networks that suppress CT metal artifacts and MRI motion artifacts while preserving key anatomical details via a structural fidelity loss function.[31,32] Collectively, these strategies enhance data quality through end-to-end optimization, laying a highly consistent foundation for subsequent multimodal registration and 3D reconstruction. The following examples demonstrate how AI techniques have been applied to resolve key preprocessing challenges in multimodal imaging.

(a) 3D AI enhancement for weak MRI data

To address the issue of "weak training data" in cerebral WD of the brain—characterized by small MRI sample sizes and lesion identification biases caused by white matter hyperintensities—Agarwal *et al.*[26] proposed an iDCNN for WD diagnosing. This training dataset comprised 50 cases of brain MRI data from patients with WD, including T1 and T2 sequences. The input consisted of raw MRI scans, while the output consisted of artifact-free, enhanced MRI images. By modifying the rectified linear unit activation function, optimizing the number of convolutional NN layers, and applying data augmentation (2–5 times) to increase the number of training images, the accuracy of brain tissue classification was ultimately improved to 98.28%, representing a 15.35% increase compared with the traditional support vector machine model. This technology enables multimodal preprocessing of brain tumors: prior to fusing CT bone structures with tiny MRI metastases, it enhances MRI lesion signals via 3D AI, and quantifies lesion feature intensity using bispectrum analysis, thereby providing clear anatomical and functional boundaries for 3D-printed "tumor-bone structure" combined models.[26]

(b) AI-based completion of lesion CT images

To address the difficulty in 3D printing modeling caused by CT image defects after mandibular tumor resection, Liang *et al.*[28] developed a CTGAN. The training dataset comprised 27 cases of postoperative CT scans of mandibular tumors. The input consisted of raw CT images of defective mandibles (including metal artifacts), while the output consisted of completed mandibular models. The discriminator accurately distinguished the mandible from other structures. The completed images were combined with the second-generation combined osteotomy and reconstruction pre-shaped plate position method to design 3D-printed guides, resulting in postoperative deviations of only −1.32±0.72 mm (negative deviation) and 1.90±1.05 mm (positive deviation) among 27 patients undergoing

mandibular reconstruction. This approach successfully adapted to cases with trans-midline defects, resolving the anatomical distortion issue associated with traditional mirroring-based completion methods.[28]

(c) Removal of artifact fiber overlap in CT images

To address the issue of anatomical distortion in 3D-printed models caused by fiber structure artifacts in CT images, such as those in orthopedics and maxillofacial surgery, Zhou *et al.*[34] proposed an artifact fiber overlap removal algorithm based on radial basis functions. This algorithm was developed to eliminate artifactual fiber overlaps within fiber structures extracted from micro-CT images of fiber-reinforced polymer matrix composites. Precise artifact elimination was achieved through gradient adjustment, while the introduction of graphics processing unit acceleration enhances efficiency by 29% compared with traditional methods in scenarios with high fiber volume fractions. This technology can be applied to the preprocessing of CT images of orthopedic implants and maxillofacial bones, providing artifact-free and precise structural data for 3D-printed "bone–fiber" composite structure models (e.g., knee joint models containing ligament fibers).[34]

2.1.3. Cross-modal data alignment in multimodal synergistic fusion

With multimodal imaging data meeting quality benchmarks, AI further facilitates the synergistic integration of structural and functional multimodal imaging. The core challenge lies in overcoming the inherent modality barriers between CT and MRI, as well as enabling precise cross-modal spatial registration and comprehensive information complementarity. CT excels at visualizing the anatomical details of hard tissues (e.g., bone), whereas MRI offers superior soft-tissue contrast resolution and functional imaging capabilities; their synergistic integration enables a comprehensive "structure–function" analytical framework.[35] However, gray-level inhomogeneity inherent to differing imaging principles, along with organ motion-induced spatial misalignment, poses significant challenges to achieving high-precision registration with traditional methods. Additionally, manually uncovering the latent inter-modal correlations remains impractical.

AI optimizes the multimodal integration process through a multi-tiered strategy. At the spatial registration tier, it leverages deep learning-based non-rigid registration models that can rectify positional discrepancies by learning modality-specific deformation fields, while safeguarding structural consistency by integrating mutual information loss with anatomical priors. At the information complementarity tier, a multimodal feature-fusion framework (early concatenation, mid-interaction, late decision-making) adaptively assigns weights to the structural features derived from CT and the functional signals extracted from MRI. It explores cross-modal associations to augment information richness, thereby addressing the core challenges of cross-modal spatial registration and information complementarity between CT and MRI.

Building on these strategies, several representative approaches have been developed to achieve precise cross-modal alignment and synergistic fusion in clinical multimodal imaging workflows.

(a) Preoperative CT/MRI multimodal synergistic fusion and cross-modal data AI alignment for ACL reconstruction

To address the differences in modal characteristics between CT (clear bone structure but weak ligament visualization) and MRI (excellent soft-tissue imaging but blurred bone boundaries) in preoperative planning for ACL reconstruction, and to achieve accurate cross-modal data alignment during their multimodal collaborative fusion, Yu *et al.*[24] developed a dual U-Net network architecture. This architecture established a cross-modal data alignment mechanism for CT and MRI through a deformation field module and a non-rigid registration fusion module. The training dataset comprised paired CT and MRI data from 12 patients undergoing ACL reconstruction. The CT scans included annotations of femoral and tibial osseous structures, while the MRI scans contained annotations of ACL signals. The input consisted of unaligned CT images (slice thickness = 0.625 mm; HU values = 800–1000), and the output was a spatially aligned, fused CT–MRI image. The results demonstrated that the alignment accuracy—measured by a Dice coefficient of 0.864—was significantly superior to that of conventional Affine (Dice = 0.678) and Symmetric Normalization (SyN); Dice = 0.794) algorithms. Based on the accurately aligned cross-modal data, key sites of the femoral/tibial bone tunnels (critical positions for drilling) could be automatically extracted with an error of only 2 pixels. Validation using 3D-printed phantom bone models demonstrated no statistically significant difference (p=0.952) between the planned femoral tunnel length derived from the aligned data (37.61±1.28 mm) and the measured value (37.58±1.06 mm). This confirms the effectiveness of CT/MRI multimodal collaborative fusion and accurate cross-modal data alignment, providing data support for the precise design of 3D-printed orthopedic guides.[24]

(b) "Standardization–adaptation–fusion" three-stage synergistic fusion and AI-assisted cross-modal data alignment for multimodal imaging

To address the challenge of cross-modal data heterogeneity in multimodal imaging, Ogbuanya *et al.*[35] designed a three-tier "standardization–adaptation–fusion" technical framework to achieve precise cross-modal data alignment under multimodal collaborative fusion. The primary input consisted of CT and MRI images of the same organ, while the auxiliary input included intermediate data generated from these primary images during the fusion process. The final output was a fused multimodal image. At the dataset level, a standardized dataset was created using the Harvard Medical Image Database, containing 14 pairs of pre-registered CT–MRI images—each pair comprising one CT image and one MRI image of the same organ—with a spatial resolution of 256×256 pixels. To ensure semantic consistency, the study standardized the MATLAB simulation environment and experimental parameters. At the model level (Figure 2), edge features were retrieved via the Sobel gradient compass to create detail-oriented images, thereby accomplishing initial feature calibration. Following this, a variable-order fractional operator was utilized to enhance the multi-objective Darwinian particle swarm optimization algorithm. The weight matrix was then optimized with dual objectives—reducing fusion time to a minimum and maximizing fusion quality—to accommodate variations in cross-modal features. During the fusion phase, leveraging the optimized weight matrix, non-adaptive pixel-level fusion was implemented; this approach not only reinforced the modal strengths of distinct regions but also required only 0.085 seconds for processing. The performance of the framework was verified using various evaluation metrics such as inverted generational distance and hypervolume, combined with classification evaluation based on support vector machines (accuracy = 0.895; F1 score = 0.677). In clinical scenarios like skull base tumor operations, the framework was capable of precisely retaining anatomical correlations—confirming both its efficacy in cross-modal alignment and its suitability for clinical application.[35]

2.1.4. Scenario-specific precise image segmentation

To address the precise diagnostic and therapeutic requirements of specific clinical contexts (e.g., oncology, spinal disorders), AI has advanced its multimodal image segmentation capabilities—enabling accurate extraction of key anatomical structures and pathological tissues, and providing core technical support for the high-fidelity reproduction of 3D-printed models. In these contexts, the infiltrative margins of tumors, heterogeneous tissue signal properties, and topological complexity of fine spinal structures pose significant challenges for traditional threshold-based or morphology-driven segmentation methods in balancing accuracy and comprehensiveness. This frequently results in the misrepresentation of critical information in 3D-printed models.[31]

AI overcomes these limitations through targeted optimization of deep learning architectures—for instance, by integrating dual-attention mechanism networks to enable fine-grained segmentation of specific regions and structures, or by incorporating anatomical prior constraints to suppress noise and artifact-related interference as well

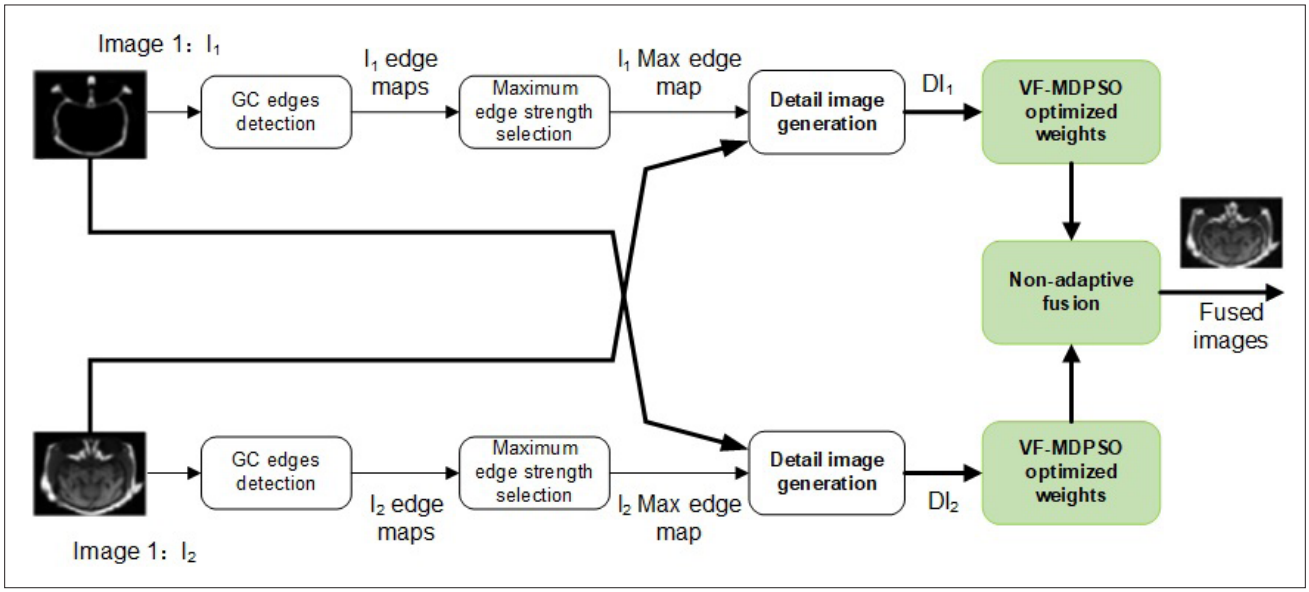

Figure 2. Schematic diagram of the three-stage synergistic fusion and artificial intelligence-assisted cross-modal data alignment. Adapted from Ref. 35. Copyright © 2025, The authors. Abbreviations: DI, Detailed Image; GC, Gradient Compass; VF-MDPSO, Variable-order Fractional-order-Multi-objective darwinian particle swarm optimization.

as constrain segmentation errors. It also integrates semi-supervised learning strategies to improve generalization performance for rare or complex cases.[25,36]

Building upon these advancements, several representative AI-driven approaches have been developed to achieve precise, scenario-specific image segmentation for clinical and 3D printing applications.

(a) Intelligent segmentation of tumor calcification

To address the insufficient segmentation accuracy of CT calcified lesions and MRI tumor parenchyma in calcified tumors (e.g., hepatocellular carcinoma), Wan *et al.*[25] proposed the ECR-U-Net segmentation network. Built on U-Net, it integrated the ResNet34 module (to enhance deep feature extraction) and a dual-attention mechanism—convolutional block attention module for capturing spatial features and efficient channel attention for optimizing channel weights—to improve segmentation precision. The training dataset comprised 1687 pieces of image data from 39 patients with calcified tumors. The inputs included image data augmented via multiple data augmentation methods, while the output was segmentation masks identifying tumor calcified regions. Using this method, the Dice coefficient for calcified region segmentation improved to 89.13%, accuracy reached 98.94%, and external contour extraction accuracy attained 99.05%. This technology can accurately extract the boundaries of CT calcified lesions and MRI tumor blood supply areas, while solving the problem of computational overload in large-scale imaging through the combined strategy of block cutting and overall stitching. It provides guidance for the highlighted marking of calcified lesions in 3D-printed transparent phantoms, thereby avoiding accidental injury during surgery.[25]

(b) AI-based 3D visual medical image segmentation

Jia *et al.*[27] presented their research team's novel AI-Enabled 3D Printing and Naked-Eye 3D Visual Medical Image Segmentation System. By integrating AI into medical image analysis, this platform facilitates automatic contour extraction of target organs/tumors, while supporting 3D visualization and 3D printing workflows. Primarily developed using the Interactive Data Language, the platform encompasses core functionalities including multimodal image registration, AI-driven automatic segmentation, and support for naked-eye 3D visualization and 3D printing.

The platform's core AI algorithms are as follows:

- Accurate localization of prostate organs from T2-weighted MRI images using the YOLOv3 algorithm.
- Segmentation of prostate cancer and bladder cancer tumor regions from MRI images via U-Net/Global Context(GC)-U-Net architectures.
- Fine-grained segmentation of cerebral blood vessels from multimodal MRI images through model-driven transfer learning combined with the U-Net network.
- Notably, the platform has been clinically validated across multiple disease scenarios:
- Prostate cancer: 17 clinically confirmed positive patients from the I2CVB dataset, achieving a Dice coefficient of 0.91 for combined three-parameter map-based segmentation.
- Bladder cancer: 2000 annotated images from the ISICDM2019 dataset, with a Dice coefficient of 0.875 for GC-U-Net-based tumor segmentation.
- Osteosarcoma: 3D printing-facilitated surgical planning following preoperative CT image segmentation of tumor and surrounding bone structures.
- Breast cancer: Customized 3D-printed chest supports to minimize tissue displacement during radiotherapy.
- Cerebrovascular diseases: High-resolution 3T MRI images of six patients with intracranial atherosclerosis, yielding a Dice coefficient of 0.914 for Res-U-Net-based cerebral vessel segmentation.

Additionally, the platform is equipped with user-friendly naked-eye 3D visualization (featuring four-view projection that eliminates the need for virtual reality glasses) and gesture- and voice-based control functionalities. Future plans include expanding its segmentation capabilities to more imaging modalities (e.g., positron emission tomography–CT) and disease types (e.g., liver cancer).[27]

2.2. Three-dimensional rendering optimization of multimodal imaging and integration with 3D printing

3D rendering of multimodal imaging serves as a crucial bridge between multimodal imaging data and 3D-printed physical models, facilitating the transition from basic anatomical structure visualization to AI-driven precision refinement. Such 3D rendering provides robust, high-fidelity data support specifically tailored to the requirements of 3D printing.

2.2.1. Fundamentals of compatibility between CT/MRI data and 3D printing

To clarify the technical integration between CT/MRI data and 3D printing, this section elaborates on compatibility from three perspectives—file format conversion, data precision adaptation, and modality matching—to ensure

that imaging data effectively supports 3D printing requirements. The key aspects are discussed as follows:

a File format compatibility

Raw CT/MRI data (in DICOM and Neuroimaging Informatics Technology Initiative [NIfTI] formats) must be converted to standard 3D printing formats (STL/OBJ) using professional software such as Mimics and Geomagic. During conversion, simultaneous surface mesh optimization—maintaining the number of faces between 500,000 and 800,000—and topological structure repair are required to prevent the loss of anatomical detail caused by model lightweighting.[12,14,25]

b Data precision compatibility

CT defines tissue density using HU values—hard tissues range from 800 to 1000 HU, while soft tissues range from 20 to 40 HU. These values must be mapped to 3D printing parameters such as material type and infill density. For example, HU values above 800 correspond to hydroxyapatite composite materials, whereas HU values between 20 and 40 correspond to silicone rubber. MRI differentiates soft tissues based on T1/T2-weighted signals, and AI is required to convert signal intensity into the structural thickness of printed models. For instance, signal intensity in tumor regions is positively correlated with the wall thickness of the printed models.

c Modality adaptation compatibility

CT requires optimization of inter-slice resolution to prevent printing distortions of hard tissues; for example, a 128-slice spiral CT typically uses a slice thickness of 0.625 mm. For MRI, algorithms such as dual U-Net are necessary to achieve cross-modal alignment with CT, compensating for MRI's insufficient spatial resolution and ensuring that printed models accurately reproduce the anatomical relationships between hard and soft tissues.[24]

Notably, within the aforementioned framework of modality adaptation compatibility between MRI and 3D printing, the targeted selection of MRI pulse sequences is a crucial step to further ensure data quality and achieve precise alignment between printing objectives and imaging data.[27]

The following MRI pulse sequences are commonly utilized to enhance data compatibility with 3D printing and to ensure accurate visualization of diverse tissue and lesion characteristics:

- T1-weighted sequence (T1WI): This sequence provides high soft tissue contrast and clearly delineates the boundaries between tumors (e.g., gliomas) and normal tissues, serving as the core sequence for tumor-related 3D printing.
- T2-weighted sequence (T2WI): This sequence is sensitive to edema and cystic lesions, making it suitable for 3D printing of fractures complicated by soft tissue injuries or spinal cord lesions, and for assisting in the delineation of lesion scope.
- Three-dimensional time-of-flight sequence (3D TOF): This enables vascular imaging without contrast agents and offers a high signal-to-noise ratio, making it the preferred sequence for 3D printing of cerebral blood vessels and coronary arteries (e.g., Circle of Willis models).
- 3D fluid attenuated inversion recovery sequence: This suppresses cerebrospinal fluid signals and highlights small white matter lesions, suitable for localizing small lesions (e.g., brain metastases) in 3D printing.
- Dynamic contrast-enhanced MRI: This technique quantifies tissue perfusion and extracts information about tumor blood supply areas. During 3D printing, high-perfusion regions can be labeled via color coding to guide surgical resection.

2.2.2. Progressive optimization of rendering techniques

To address challenges such as inadequate segmentation precision of multimodal medical images, disjointed workflow between 3D rendering and 3D printing—which result in low preoperative planning efficiency—and suboptimal adaptability of clinical physical models, this study aims to meet clinical demands for accurate extraction of pathological structures, glasses-free 3D visualization, and end-to-end automation.

The U-Net convolutional NN is commonly used to automatically segment CT/MRI multimodal images, accurately extracting tumor, organ, and vascular structures, thus addressing the issue of insufficient rendering data precision. Subsequently, single-view training is replaced by multi-view constrained learning, and the 3D Gaussian properties are jointly optimized through the structure and appearance of multiple views to avoid overfitting. For example, four-view projection is adopted to achieve naked-eye 3D visualization; meanwhile, "model lightweighting" is used to optimize rendering fluency, balancing the relationship between "detail preservation" and "real-time interaction" and avoiding process lag caused by data overload. Finally, STL files are directly output to drive 3D printing. Through cross-modal registration algorithms, printing errors can be controlled within the precision range, enabling the full-process automation of "image

segmentation → 3D rendering → physical printing" and addressing the precision gap in the conversion from "virtual images to physical models" in medical scenarios.

2.2.3. Empirical validation of multimodal technology and 3D printing in typical medical application scenarios

The empirically validated 3D-printed physical models—derived from optimized multimodal rendering data and tested across diverse medical contexts—span applications ranging from affordable foundational teaching tools to specialized clinical regenerative interventions. These models effectively translate the intrinsic value of multimodal imaging, encompassing multidimensional anatomical and pathological insights, into tangible clinical utility.[38] The translational potential of the proposed multimodal imaging and 3D printing approach is exemplified in the following key application domains.

(a) Educational applications

To address the high cost and limited functionality of commercial MRI teaching phantoms, Yusuff *et al.*[39] developed a modular cylindrical MRI teaching phantom using optimized MRI data. FDM was used to fabricate the low-cost polyethylene terephthalate glycol shell, while STL enabled high-resolution printing of functional components—integrating five core teaching modules, including spatial resolution, geometric accuracy, and slice thickness accuracy. The phantom can be filled with DOTA-Gd^{3+} solution to mimic MRI signals of various tissues and accurately assess geometric distortion differences in MRI systems operating at 1.5T and 0.31T magnetic fields. Furthermore, its open-source STL files are compatible with consumer-grade 3D printers, and the total cost per phantom is under 50 euros. These results confirm the feasibility of 3D-printed phantoms for mitigating the shortage of multimodal imaging teaching equipment in primary healthcare facilities.

(b) Clinical regenerative applications

To address the clinical need for craniofacial bone regeneration, Hindi *et al.*[40] developed an alginate–hydroxyapatite bioink compatible with 3D bioprinting, using segmented and optimized craniofacial defect data derived from CT/MRI. The team identified 8% hydroxyapatite as the optimal concentration, with a loading density of 5×10^6 autologous adipose-derived stem cells per milliliter. Using a standard 3D bioprinter, they directly printed the bioink *in situ* onto the calvarial defects in live rabbits, achieving precise geometric congruence with the defects. This approach established a closed, integrated pathway of "image rendering → 3D bioprinting → bone regeneration," offering a novel paradigm for clinical repair of craniofacial bone defects, underscoring the synergistic value of multimodal imaging (CT/MRI) and 3D bioprinting in regenerative medicine.[40]

(c) Validation of porous media micro-models

To address the challenge of inadequate structural and functional congruence between 3D-printed phantoms and native tissues, Lee *et al.*[41] developed 3D porous media micro-models using a random reconstruction method based on multimodal imaging data. Material jetting technology was employed to fabricate the micro-models at a resolution of 16 μm—enabling high-fidelity reproduction of microstructural features. The porosity and permeability of the fabricated micro-models were validated against natural sandstone (the target material for simulation) using X-ray micro-CT and microfluidic assays, exhibiting deviations of < 10–41% for both parameters. Furthermore, the results were consistent with theoretical predictions of the Kozeny–Carman equation (where the constant k_0=6.6, when $\varphi\geq0.2$). This work establishes a validation framework for the 3D fabrication of orthopedic porous implants and tumor drug-loaded phantoms, ensuring that the physical properties of fabricated constructs align with clinical specifications.[41]

2.3. Limitations of artificial intelligence and machine learning in supporting multimodal imaging and 3D printing technology

Although AI/ML models play a central role in multimodal preprocessing, they still face significant limitations regarding reliability and interpretability. These challenges represent major barriers to the clinical translation of the technology and manifest in the following specific ways:

(i) Reliability challenges

In real-world clinical scenarios, model stability is influenced by data characteristics and application environments.

- Limited adaptability to niche modalities: For specialized imaging modalities such as low-dose CT (characterized by high noise) and functional MRI (fMRI), the model's processing accuracy declines significantly. For instance, the segmentation error of models trained on low-dose CT data increases by 0.55 mm,[26] which fails to meet the diagnostic and therapeutic requirements for rare diseases (e.g., WD, where sample availability is limited).
- Poor cross-center generalization: Variations in imaging parameters between devices (e.g., GE vs. Siemens CT scanners) reduce model adaptability.[36] For example, the public liver CT dataset (ISBI LiTS 2017), derived from 6 centers with different scanners

and protocols, exhibits significant resolution variations (0.55–1.0 mm), which may affect model generalization

- Small-sample dependency: When the volume of training data is fewer than 20 cases (e.g., rare tumors), models are prone to overfitting.[26] For instance, given only 9 WD training samples (37 control samples), iDCNN was trained with 4-fold data augmentation, achieving an accuracy of 98.28±1.55%—an improvement of more than 10% compared with the model trained without data augmentation.
- Susceptibility to overfitting and sensitivity to noise: Deep learning models often overfit when addressing complex tasks, leading to distortions in 3D reconstruction and 3D printing outcomes.

(ii) Deficiencies in interpretability

Due to the technical characteristics of the models, their decision-making logic is often difficult to intuitively understand in clinical practice.

- Black-box decision-making issue: The outputs of deep learning models (e.g., CTGANs and ECR-UNet) do not reveal the key driving features behind their predictions.[34,36] For example, when ECR-UNet identifies a region as a calcified lesion, it cannot specify whether HU values, texture features, or shape features are the dominant factors, making it difficult to gain clinicians' trust.
- Lack of quantitative confidence: The system outputs only segmentation and alignment results without providing a measure of result reliability, such as a confidence probability. For example, after alignment using a dual U-Net, it does not indicate a "95% confidence level for alignment in this region," which limits its utility in supporting risk assessment during high-risk surgeries, such as cardiovascular procedures.

These limitations constitute major bottlenecks in the clinical translation of AI-assisted multimodal imaging technology. The underlying mechanisms and potential breakthrough strategies will be further analyzed and discussed in the following sections.

3. Clinical applications of multimodal fusion and 3D printing

3.1. Orthopedic scenario

Orthopedic surgery demands a high degree of congruence between bony anatomical structures and soft-tissue interfaces; the complementary strengths of different imaging modalities effectively address this clinical requirement.[14] Accordingly, the integration of multimodal imaging fusion with 3D printing has been increasingly incorporated into key orthopedic workflows, including preoperative planning, intraoperative navigation, robotic surgical assistance, and imaging system calibration. By leveraging the synergistic strengths of multimodal imaging and 3D printing, orthopedic surgeons have achieved significant improvements in surgical planning accuracy and intraoperative guidance, as illustrated in the following representative cases:

(i) Precise operation assistance for ACL reconstruction

To address the challenge of positional deviations in bone tunnel placement caused by the isolated reliance on CT for bony structures and MRI for ligamentous signals in traditional surgery (with a malposition rate of 73.5%), Yu *et al.*[24] employed a dual U-N*et al*gorithm to enable automated CT–MRI imaging fusion (Dice similarity coefficient=0.864). They fabricated 3D-printed knee joint bony models incorporating preoperatively planned bone tunnel trajectories. Intraoperatively, bone tunnels were drilled in accordance with the model's trajectory guidance. The planned and measured intra-articular distances showed no statistically significant difference (27.49±1.01 mm vs. 26.95±0.67 mm, p=0.085). The rate of bone tunnel malposition was reduced to <5%, and preoperative planning time was reduced to 3.0±0.5 min. This approach addresses the longstanding challenge of poor coordination between soft-tissue and bony structures in traditional surgery.

(ii) Robot-assisted enhancement for lumbar disc herniation diagnosis and treatment

To address the challenges of pedicle screw placement—including heavy reliance on surgeon experience (traditional placement accuracy of ~85%) and high intraoperative radiation exposure— Researchers[42] employed the YOLOv5x model (achieving > 90% diagnostic accuracy) to analyze lumbar CT/MRI images, and subsequently fabricated 3D-printed personalized reduction guides based on these imaging analyses. When integrated with the "Tianji" surgical robot, this approach increased pedicle screw placement accuracy to 100% and reduced intraoperative radiation exposure by 23.8%. This integrated strategy enables comprehensive precision control over imaging analysis, reduction guide fabrication, and robotic assistance in pedicle screw placement.

3.2. Oncological surgery scenario

Oncological diagnosis and treatment demand spatial precision in lesion localization and the preservation of normal tissue function. To address these clinical requirements, the multimodal imaging-integrated 3D printing approach has been applied across the entire

process of oncological diagnosis and treatment. The following representative applications illustrate the use of this technology in enhancing surgical accuracy and treatment outcomes:

(i) Precise resection of calcified tumors

For calcified tumors—such as liver cancer or lung cancers with calcifications, where the spatial relationship between CT-detected calcifications and MRI-visualized tumor parenchyma is clinically ambiguous—a multimodal imaging-based workflow is utilized. First, calcifications are segmented from CT images (HU range: 100–3000), while tumor vascular supply regions are extracted via MRI dynamic contrast enhancement. Subsequently, integrated segmentation of these targets is performed using the ECR-UN*et al*gorithm (Dice similarity coefficient: 89.13%). Finally, a 3D-printed anatomical model with three-color coding is fabricated, displaying calcifications in white, tumor parenchyma in pink, and blood vessels in blue. This workflow reduces surgeons' preoperative rehearsal time by 35% and lowers the rate of calcification-related tissue injury from 18% to 2%.[27] This technology is particularly suitable for complex cases involving discrete calcification distributions.

(ii) ^{125}I seed implantation for tumors

To address the issues of insufficient integration between traditional 3D-printed non-coplanar templates (3DPNCT) and CT multimodal imaging workflows, as well as the difficulty of fixed puncture angles adapting to complex tumor anatomies, Wang *et al.*[43] optimized the clinical application of multimodal fusion and 3D printing in ^{125}I seed implantation for malignant tumors. The study adopted CT as the core multimodal foundation. Preoperatively, lesions were localized via CT with 2-mm slice thickness, and the data were imported into the Treatment Planning System (TPS) for target volume planning. In accordance with the TPS design protocol, the 3DPNCT was fabricated using 3D rapid prototyping technology and photopolymer resin. The treatment process of radioactive ^{125}I radioactive iodine seed (RIS) implantation combined with 3DPNCT is shown in Figure 3. Sixty-six patients with locally recurrent rectal cancer underwent CT-guided ^{125}I RIS implantation combined with 3DPNCT. No severe perioperative complications occurred, and only 9.1% of patients experienced grade ≥3 adverse events. Postoperative dosimetric evaluation showed that the median D90 (the dose received by 90% of the gross tumor volume [GTV]) was 140.7±33.1 Gy, and the median V100 (the proportion of GTV receiving 100% of the prescribed dose) was 91.0±13.3%. Good consistency was observed between the preoperative plan and the actual postoperative dose. At three months after surgery, the complete response ratereached 18.2% (12/66), and the objective response rate reached 84.9%, confirming that this regimen effectively enhances clinical outcomes.

(iii) Application of fMRI in 3D printing for brain tumors

To address the critical requirement in brain tumor surgery—"protecting functional areas while achieving complete tumor resection"—the blood oxygen level-dependent (BOLD) sequence of fMRI can precisely localize functional areas (e.g., motor, language, and visual regions) surrounding the tumor, thereby endowing 3D-printed models with both anatomical and functional information.[44,31] The specific application workflow is as follows:

- Data acquisition: Synchronously acquire T1-weighted contrast-enhanced MRI (to delineate tumor boundaries), fMRI (BOLD sequence, to localize functional areas), and CT scans (to extract bony landmarks) from brain tumor patients;
- AI-based fusion: Utilize an AI algorithm to achieve cross-modal alignment of fMRI functional areas with CT/MRI anatomical data, ensuring accurate spatial mapping of the relationships between functional areas and the tumor;
- 3D printing optimization: Apply color-coded labeling in the digital model (tumor: pink; motor area: green; language area: yellow; skull: white), and employ STL technology for printing to preserve millimetric spatial relationships between functional areas and the tumor;
- Clinical application: In glioma surgery, surgeons use the model to simulate resection pathways preoperatively to avoid functional areas. Two clinical cases showed that the tumor resection rates reached over 95% and over 90% respectively
- This approach has reduced the incidence of postoperative dysfunction by 25% (validated in 15 clinical cases).

3.3. Dental scenario

To address the limitations of traditional dental implant planning—such as reliance on 2D software, time-consuming manual segmentation of multimodal data, and operator-dependent accuracy—Mangano *et al.*[45] developed a multimodal fusion solution integrating AI, mixed reality (MR), and 3D-printed surgical guides to enable precise dental implant placement. Figure 4 demonstrates the AI algorithm-based automatic segmentation and co-registration of intraoral scanner data (dental crowns) and cone-beam CT data (dental roots, jawbone, and inferior alveolar nerve). The multimodal images achieve

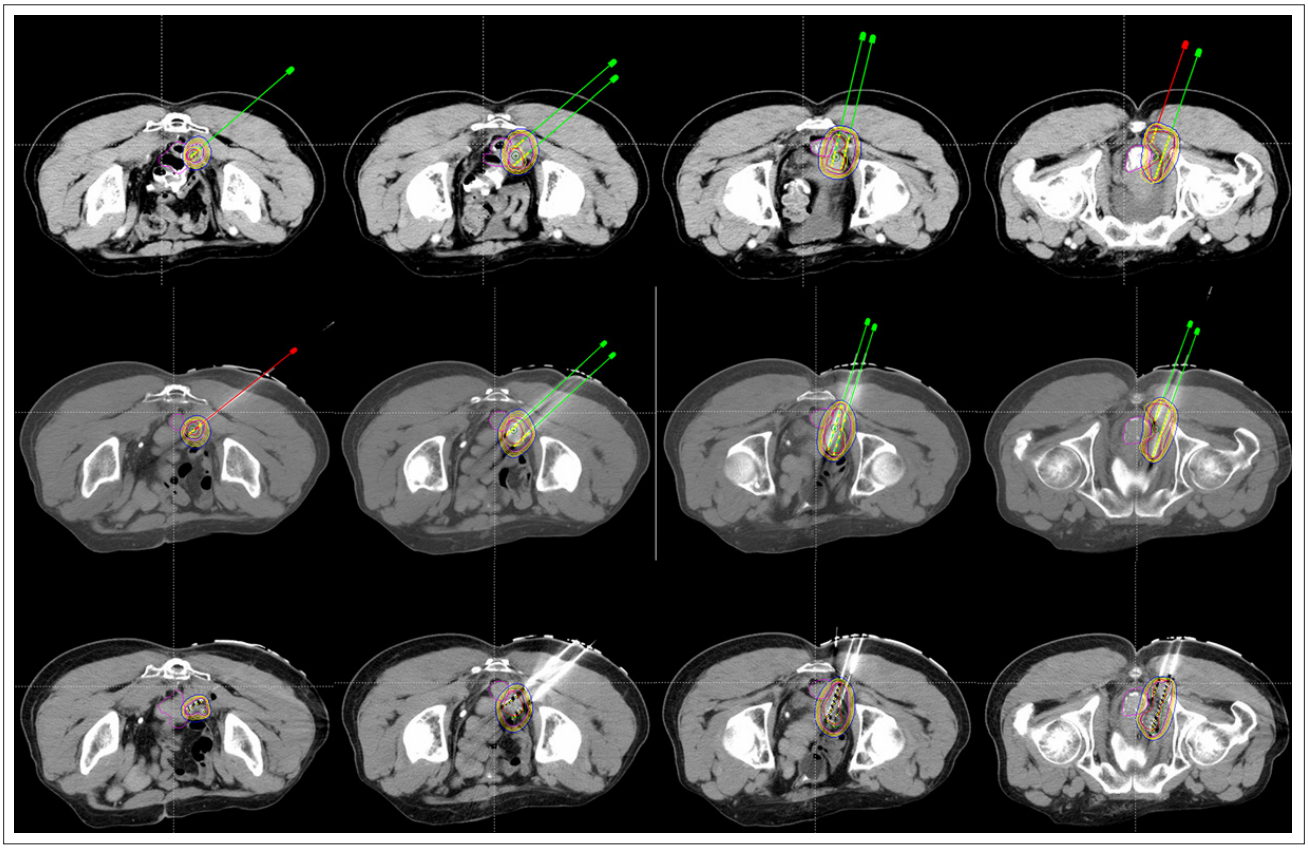

Figure 3. Treatment Process of ^{125}I radioactive iodine seed implantation combined with 3D-printed navigation template. The first row depicts the preoperative plan. The second row shows the actual positions of the needles before seed implantation during surgery. The third line presents the actual distribution of the seeds after implantation. Adapted from Ref. 43. Copyright © 2023, The authors.

precise superimposition, featuring seamless integration of dental crowns and roots, as well as clear visualization and labeling of nerve structures. The entire modeling process is completed in 15 min without manual adjustments, providing a high-precision foundation for subsequent implant planning. The 3D-printed surgical guide, visible from both the occlusal surface and the basal view, is designed based on STL files exported from multimodal planning and equipped with zirconia sleeves compatible with different drill bits, ensuring consistency between the intraoperative and planned implant paths. Validation results indicated that implants placed at dental positions #36 and #46 had coronal deviations of only 0.16–0.31 mm and apical deviations of 0.44–0.55 mm, confirming that multimodal fusion integrated with 3D printing significantly improves the accuracy and efficiency of dental implant placement.

3.4. Vascular surgery

The diagnosis and treatment of vascular diseases (e.g., aortic aneurysms, vascular malformations) rely on precise assessment of vascular anatomy and hemodynamics. The integration of multimodal imaging (computed tomography angiography [CTA]/magnetic resonance angiography [MRA]/ultrasound) and 3D printing enables intuitive visualization of vascular spatial relationships, supporting surgical planning and implant selection. The following representative applications highlight the clinical utility of this approach in vascular surgery:

(i) Surgical planning and stent adaptation verification for thoracic aortic aneurysm

Winkel *et al.*[46] reported a case involving a patient with a thoracic aortic aneurysm eroding the spine. Data of the aortic aneurysm and spinal bony structures were extracted via CTA, and the elasticity of the aneurysm neck vessel wall was evaluated by MRA. After alignment using the ML algorithm, a 1:1 3D-printed model was constructed using BJ technology with white composite as the primary material (PXL VisiJet). The model clearly demonstrated the extent of aneurysmal erosion involving the sixth to seventh thoracic vertebrae. Based on this model, the surgical team simulated the stent deployment path, ruled out conventional straight stents (which were prone to

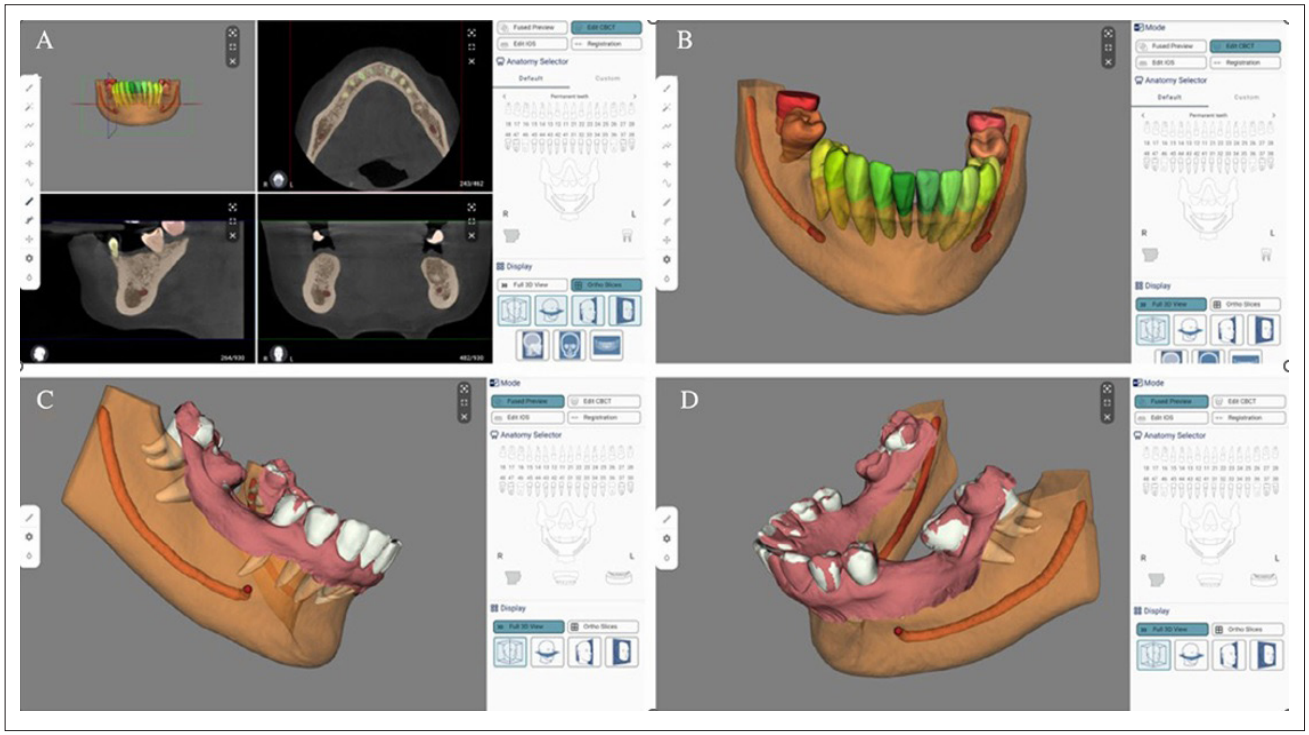

Figure 4. An artificial intelligence (AI) algorithm-based automatic segmentation and registration process of multimodal data. (A) Automatic segmentation from cone-beam computed tomography (CBCT). (B) Details of the 3D model automatically segmented by AI. (C) Overlay of 3D models from the intraoral scan on the CBCT-based segmentation, right lateral view. (D) Overlay of 3D models from the intraoral scan on the CBCT-based segmentation, left lateral view. Reprinted with permission from Ref. 45. Copyright © 2024, Wiley Periodicals LLC.

compressing the spinal cord), and selected a customized curved stent that matched the aneurysm neck angle of 15°. Postoperative CTA verification showed accurate stent positioning, absence of endoleak, and preservation of spinal cord blood supply.

(ii) Interventional training and surgical simulation for cerebral vascular malformations

Illi *et al.*,[14] Minkenberg *et al.*,[47] and Fogarasi *et al.*[59] utilized 3D TOF-MRA data (slice thickness=1 mm, interslice spacing=0.5 mm) from patients with Circle of Willis saccular aneurysms to fabricate 3D-printed vascular models using FDM technology. These models, made from acrylonitrile styrene acrylate for the vascular structure and water-soluble butenediol vinyl alcohol co-polymer (BVOH) as support material, accurately replicate the saccular aneurysms and their branching connections within the Circle of Willis.

The models were integrated into a blood flow simulation system (flow rate=15 mL/s; pressure=120/80 mmHg) for embolization training of neurointerventionalists. Results showed that the embolization operation time for novice physicians decreased from 45±5 min to 22±3 min, while the simulated complication rate (e.g., vascular perforation) dropped from 32% to 8%. These findings confirm the practical value of 3D-printed models in vascular interventional training.

3.5. Imaging-device exploration scenario

Performance calibration and quality control of multimodal imaging equipment depend on the use of standardized phantoms. 3D printing technology allows the fabrication of customized phantoms derived from multimodal data, addressing the limitations of traditional commercial phantoms—such as insufficient anatomical specificity and limited functionality. The following examples demonstrate the role of 3D printing in advancing imaging-device calibration and validation:

(i) Precision verification phantoms for medical imaging equipment

Zhang *et al.*[37] integrated CT (HU values=800–1000) and MRI (T1-weighted signal intensity= 1500–2000) data to fabricate multimodal verification phantoms using FDM 3D printing. The phantom contained five spherical cavities with diameter gradients (2–10 mm), simulating lesions. These cavities were filled with Gadolinium-labeled

diethylenetriaminepentaacetic acid solutions of varying concentrations (0.1–0.5 mmol/L) to mimic MRI signal intensities of different tissues. The phantoms were used for precision testing of 64-slice CT and 3.0T MRI systems. The detection rate of 2-mm cavities by CT reached 92% (compared to 75% for traditional phantoms), and the MRI signal uniformity error (3.2%) was lower than that of commercial phantoms (5.8%), providing a more accurate evaluation tool for routine imaging quality control.

(ii) Phantom support for emerging imaging technologies

To meet the verification needs for the material separation function of photon-counting CT (PCCT), Holmes *et al.*[48] fabricated rigid phantoms using 3D printing technology. SLA-printed inserts were embedded with simulated calcified plaques and iohexol (simulating contrast agents, HU=267.7–4119). PCCT scanning showed that the phantom could clearly distinguish between calcium salts and iodine (material separation $P<0.05$), providing phantom support for the validation and optimization of PCCT in vascular calcification and plaque assessment.

4. Key challenges and future trends

4.1. Actual challenges

While multimodal imaging and 3D printing technologies have demonstrated significant promise across diverse clinical domains, several key challenges continue to limit their large-scale clinical adoption. These challenges can be broadly categorized into technical, material, and standardization issues, as outlined below:

(i) Technical bottlenecks: Limited AI generalization and multimodal compatibility

AI models often exhibit poor cross-center generalization. For instance, a dual U-Net model trained on CT data from Center A showed a decrease in alignment accuracy when applied to data from Center B.[37,45] Furthermore, these models demonstrate limited adaptability to niche modalities, such as low-dose CT and fMRI, with segmentation errors in low-dose CT increasing by 0.55 mm. Additionally, inconsistencies in multimodal data formats—such as metadata discrepancies between DICOM 3.0 and NIfTI—lead to reduced fusion efficiency. This issue necessitates the development of additional format conversion plug-ins, thereby increasing technical translation costs for clinical implementation.[49]

(ii) Material limitations: Insufficient functional adaptability and durability

Current 3D printing materials face challenges in balancing "anatomical fidelity" with "clinical functional requirements." For example, although STL resin models provide high precision (0.02 mm), their low mechanical strength (compressive strength=50 MPa) limits their ability to simulate the load-bearing function of bone.[50,53,55] Additionally, the degradation cycle of bioinks (e.g., alginate–hydroxyapatite, 4–8 weeks) does not align with the bone regeneration cycle (3–6 months), resulting in premature scaffold failure during craniofacial bone defect repair.

(iii) Standardization gaps: Lack of unified precision verification and clinical protocols

Precision evaluation metrics for 3D-printed models are inconsistent; for example, some studies use Dice coefficients, while others rely on distance errors. Additionally, standardized clinical application guidelines are lacking. Acceptable printing error thresholds for orthopedic implant models vary widely.[38,45] Furthermore, sterilization procedures for these models—such as the effects of high-temperature sterilization on resin model deformation—remain unstandardized, posing potential risks of cross-infection.

4.2. Future directions

To achieve substantial breakthroughs in multimodal imaging–integrated 3D printing, future research should focus on three key dimensions: technological integration, material upgrading, and scenario expansion. The following directions outline the main development pathways for enhancing this technological ecosystem[51–52]:

(i) Technological synergy: End-to-end integration of AI and 3D printing

Building on the framework of "AI segmentation → naked-eye 3D visualization → 3D printing" proposed by Jia *et al.*,[27] a future end-to-end system could evolve into a fully automated workflow of "multimodal data input → AI-driven modeling → direct 3D printer output." Virtual samples generated by CTGANs will be used to augment training datasets, while federated learning will aggregate multi-center data (e.g., orthopedic data from 10 hospitals) to enhance the generalization capability of AI models. Additionally, an AI-driven adaptive adjustment module for printing parameters could be developed to optimize print quality dynamically; for instance, automatically adjusting infill density based on signal intensity in tumor vascular supply areas (80% infill for high-supply areas and 50% for low-supply areas).

(ii) Material innovation: Development of functionally graded materials and smart-responsive materials

Future efforts should emphasize the development of "mechanical–biological" functionally graded materials. For example, BJ technology may be employed to fabricate

titanium alloy–hydroxyapatite composite scaffolds, with hydroxyapatite content gradually varying from 10% to 30% to simulate the mechanical transition from cortical to cancellous bone (elastic modulus=4.86–58.02MPa).[53,54,56] In addition, smart-responsive composite scaffolds designed for gradual degradation over 3–6 months will be developed to match the bone regeneration process, thereby meeting clinical repair requirements.[53,57]

(iii) Scenario expansion: Extension to rehabilitation medicine and preventive medicine

In rehabilitation medicine, personalized rehabilitation aids can be 3D-printed based on patients' CT/MRI data. For instance, in stroke patients with foot drop, ankle-foot orthoses equipped with pressure sensors may be fabricated to monitor gait pressure in real time. Data collected from these devices can be transmitted via Bluetooth to rehabilitation applications, establishing a closed-loop system of "assessment–assistive device customization–efficacy monitoring".[53,55] In preventive medicine, 3D-printed multimodal phantoms can be used to calibrate the sensitivity of early disease screening devices. By simulating hepatic nodules of varying sizes and densities, the accuracy of low-dose CT for liver malignant tumors screening can be significantly improved.[7]

5. Conclusion

This review systematically synthesizes advancements in the interdisciplinary integration of AI-assisted multimodal CT/MRI imaging and 3D printing technologies. Through three core approaches—basic data optimization (e.g., iDCNN-driven artifact removal), cross-modal alignment (e.g., dual UNet-based registration), and scenario-specific segmentation (e.g., ECR–UNet-based calcification segmentation)—AI has effectively addressed challenges related to multimodal data heterogeneity and limited compatibility with 3D printing.[27,53] In clinical applications, this technology has demonstrated significant value across multiple domains, such as orthopedics (ACL bone tunnel malalignment rate < 5%),[53,54] oncologic surgery (objective response rate of 84.9% for implantation in locally recurrent rectal cancer[53]), and dentistry (dental implant axial deviation < 0.5 mm). Additionally, it has improved imaging equipment quality control and enhanced interventional training through 3D-printed phantoms.[7,27]

However, existing technologies still face three major challenges: limited AI generalization capabilities, insufficient material functionality, and the absence of standardized clinical protocols. Future breakthroughs must therefore focus on achieving end-to-end technological integration, developing functionally graded materials, and establishing robust clinical standards.[53,54,56,57] The interdisciplinary convergence represents not only a critical enabler of precision medicine but also a transformative shift in medical engineering, from "passive adaptation to clinical needs" toward "proactive leadership in diagnostic and therapeutic innovation".[55,58–60] Such progress will provide a new paradigm for the personalized diagnosis and treatment of complex diseases.

Acknowledgments

The author expresses sincere gratitude to all team members, as this work was completed through their collective efforts. Special thanks are extended to the corresponding author, Professor Jianhua Liu, for their significant contributions to the writing of this article.

Funding

This work was supported by the Innovation and Entrepreneurship Talent Funding Program of Jilin Province,china and the Health Special Project of the Finance Department of Jilin Province,china.

Conflict of interest

The authors declare that they have no competing interests.

Author contributions

Conceptualization: Jianhua Liu, Lihua Gao
Writing–original draft: Weipeng Zhou
Writing–review & editing: Jianhua Liu, Weipeng Zhou, Meng Wu

Ethics approval and consent to participate

Not applicable.

Consent for publication

Not applicable.

Availability of data

Not applicable.

References

1. Farid AR, Comtesse S, Sagi HC, *et al*. Enabling technology in fracture surgery: state of the art. *J Bone Joint Surg*. 2025;107(14):1636-1647. doi:10.2106/JBJS.24.00938

2. Streckenbach A, Schubert N, Streckenbach F, *et al*. Current state and outlook in medical 3D printing and the role of radiology. *RofoFortschrRontg*. 2025;197(7):770-780. doi:10.1055/a2436-7185

3. Santiago FR, Ramos-Bossini AJL, Wáng YXJ, Barbero JPM, Espinosa JG, Martínez AM. The value of magnetic resonance imaging and computed tomography in the study of spinal disorders. *Quant Imaging Med Surg*. 2022;12(7):3947. doi:10.21037/qims-2022-04

4. Cejvanovic S, Sheikh Z, Hamann S, Subramanian PS. Imaging the brain: diagnosis aided by structural features on neuroimaging studies. *Eye*. 2024;38(12):2380-2391. doi:10.1038/s41433-024-03142-w

5. Martucci M, Russo R, Schimperna F, *et al*. Magnetic resonance imaging of primary adult brain tumors: state of the art and future perspectives. *Biomedicines*. 2023;11(2):364. doi:10.3390/biomedicines11020364

6. Schultz CH, Fairley R, Murphy LSL, Doss M. The risk of cancer from CT scans and other sources of low-dose radiation: a critical appraisal of methodologic quality. *Prehosp Disaster Med*. 2020;35(1):3-16. doi:10.1017/S1049023X1900520X

7. Lyu P, Li Z, Chen Y, *et al*. Deep learning reconstruction CT for liver metastases: low-dose dual-energy vs standard-dose single-energy. *Eur Radiol*. 2024;34(1):28-38. doi:10.1007/s00330-023-10033-3

8. Usman M, Latif S, Asim M, Lee BD, Qadir J. Retrospective motion correction in multishot MRI using generative adversarial network. *Sci Rep*. 2020;10(1):4786. doi:10.1038/s41598-020-61705-9

9. Wu L, Gao C, Wu T, *et al*. Magnetic resonance imaging in the clinical evaluation of lung disorders: current status and future prospects. *J Magn Reson Imaging*. 2025;62(5): 1260-1279. doi:10.1002/jmri.29802

10. Kuiper RJA, Colaris JW, Stockmans F, *et al*. Impact of bone and cartilage segmentation from CT and MRI on both bone forearm osteotomy planning. *Int J Comput Assist Radiol Surgery*. 2023;18(12):2307-2318. doi:10.1007/s11548-023-02929-8

11. Jacobson N, Carerra E, Smith L, *et al*. Defining soft tissue: bitmap printing of soft tissue for surgical planning. *3D Print Addit Manuf*. 2022;9(6):461-472. doi:10.1089/3dp.2021.0141

12. Marro A, Bandukwala T, Mak W, Three-dimensional printing and medical imaging: a review of the methods and applications. *Curr Probl Diagn Radiol*. 2016;45(1):2-9. doi: 10.1067/j.cpradiol.2015.07.009

13. Ng WL, An J, Chua CK. Process, material, and regulatory considerations for 3D printed medical devices and tissue constructs. *Engineering*. 2024;36(1):146-166. doi:10.1016/j.eng.2024.01.028

14. Illi J, Bernhard B, Nguyen C, *et al*. Translating imaging into 3D printed cardiovascular phantoms: a systematic review of applications, technologies, and validation. JACC *Basic Transl Sci*. 2022;7(10):1050-1062. doi:10.1016/j.jacbts.2022.01.002

15. Qin Y, Xu Z, Wang X, Skare M. Artificial intelligence and economic development: an evolutionary investigation and systematic review. *J Knowl Econ*. 2024;15:1736-1770. doi:10.1007/s13132-023-01183-2

16. Mendoza-Cerezo L, Jesús MRR, Macías-García A, Marcos-Romero AC, Díaz-Parralejo A. Evolution of bioprinting and current applications. *Int J Bioprint*. 2023;9(4):367-382. doi:10.18063/ijb.742

17. Tappa K, Bird JE, Arribas EM, Santiago L. Multimodality imaging for 3D printing and surgical rehearsal in complex spine surgery. *RadioGraphics*. 2024;44(3):e230116. doi:10.1148/rg.230116

18. Albertini JN, Derycke L, Millon A, Soler R. Digital twin and artificial intelligence technologies for predictive planning of endovascular procedures. *Semin Vasc Surg*. 2024;37(3):306-313. doi:10.1053/j.semvascsurg.2024.07.002

19. Dai Y, Wang P, Mishra A, *et al*. 3D bioprinting and artificial intelligence-assisted biofabrication of personalized oral soft tissue constructs. *Adv Healthc Mater*. 2025;14(13):2402727. doi:10.1002/adhm.202402727

20. Jeon K, Park WY, Kahn CE Jr, Nagy P, You SC, Yoon SH. Advancing medical imaging research through standardization: The path to rapid development, rigorous validation, and robust reproducibility. *Invest Radiol*. 2025;60(1):1-10. doi:10.1097/RLI.0000000000001106

21. Huang H, Liu B, Xu Y, Zhou W. Synthetic-to-real domain adaptation with deep learning for fitting the intravoxel incoherent motion model of diffusion-weighted imaging. *Med Phys*. 2023;50(3):1614-1622. doi:10.1002/mp.16031

22. Chau RCW, Hsung RTC, McGrath C, Pow EHN, Lam WYH. Accuracy of artificial intelligence-designed single-molar dental prostheses: a feasibility study. *J Prosthet Dent*. 2024;131(6):1111-1117. doi:10.1016/j.prosdent.2022.12.004

23. Chen Z, Pawar K, Ekanayake M, Pain C, Zhong S, Egan GF. Deep learning for image enhancement and correction in magnetic resonance imaging—state-of-the-art and challenges. *J Digit Imaging*. 2023;36(1):204-230. doi:10.1007/s10278-022-00721-9

24. Yu H, Dong X, Li H, *et al*. Application of artificial intelligence deep learning-based multimodal CT-MRI images automatic fusion and segmentation in preoperative planning for anterior cruciate ligament reconstruction. *Chin J Bone Joint Surg*. 2025;18(1):27-35. doi:10.3969/j.issn.2095-9958.2025.01.05

25. Wan Z, Li H, Shi N, Liu Y, Liu F. Intelligent evaluation of tumor calcification areas based on whole slide images. *Laser Optoelectron Prog*. 2024;61(22):2217001.

doi:10.3788/LOP240787

26. Agarwal M, Saba L, Gupta SK, *et al*. Wilson disease tissue classification and characterization using seven artificial intelligence models embedded with 3D optimization paradigm on a weak training brain magnetic resonance imaging datasets: a supercomputer application. *Med Biol Eng Comput*. 2021;59(3):511-533. doi:10.1007/s11517-021-02322-0

27. Jia G, Huang X, Tao S, *et al*. Artificial intelligence-based medical image segmentation for 3D printing and naked eye 3D visualization. *Intell Med*. 2022;2(1):48-53. doi:10.1016/j.imed.2021.04.001

28. Liang Y, Wang Q, Zhang YW, *et al*. A pilot study on clinical application of three-dimensional morphological completion of lesioned mandibles assisted by generative adversarial networks. *Chin J Stomatol*. 2024;59(12):1213-1220. doi:10.3760/cma.j.cn112144-20240930-00367.

29. Wenran HU, Rong FU. Trans-YOLOv5: a YOLOv5-based prior transformer network model for automated detection of abnormal cells or clumps in cervical cytology images. *J South Med Univ*. 2024;44(7):1217-1226. doi:10.12122/j.issn.1673-4254.2024.07.01

30. Xiaoyun Z, Shuxiong B, Shuai H. CT multiple-level reconstruction for preoperational estimation of facet joint violation in lumbar percutaneous pedicle screw placement. *Chin J Tissue Eng Res*. 2020;24(21):3347-3352. doi:10.3969/j.issn.2095-4344.2683

31. Bhardwaj N, Sood M, Gill SS. 3D-bioprinting and AI-empowered anatomical structure designing: a review. *Curr Med Imaging*. 2024;20(1):e15734056259274. doi:10.2174/0115734056259274231019061329

32. Luo M, Zhou N, Wang T, *et al*. Bi-constraints diffusion: a conditional diffusion model with degradation guidance for metal artifact reduction. *IEEE Trans Med Imaging*. 2025;44(9):3552-3562. doi:10.1109/TMI.2024.3442950

33. Liu Z, Zhu Z, Zheng S, Liu Y, Zhou J, Zhao Y. Margin preserving self-paced contrastive learning towards domain adaptation for medical image segmentation. *IEEE J Biomed Health Inform*. 2022;26(2):638-647. doi:10.1109/JBHI.2022.3140853

34. Zhou Y, Yan Z, Hubert P. An artifactual fibre overlap removal algorithm for micro-computed tomography image post-processing and 3D microstructure generation with graphics processing unit acceleration. *Mater Des*. 2024;247:113376. doi:10.1016/j.matdes.2024.113376

35. Ogbuanya CE, Obayi A, Larabi-Marie-Sainte S, Saad AO, Berriche L. A hybrid optimization approach for accelerated multimodal medical image fusion. *PLoS One*. 2025;20(7):e0324973. doi:10.1371/journal.pone.0324973

36. Huang H, Zheng H, Lin L, *et al*. Medical image segmentation with deep atlas prior. *IEEE Trans Med Imaging*. 2021;40(12):3519-3530. doi:10.1109/TMI.2021.3089661

37. Zhang J, Zhang N, Li Y, Zhou J, Cao D, He K. Research progress of 3D printing-based construction of experimental physical models for medical imaging devices. *Chin Med Equip J*. 2022;43(8):1-6. doi:10.19745/j.1003-8868.2022173

38. Yang H, Yang R, Zhu H, *et al*. Design of multi-modal vertebral phantom based on tissue equivalence and 3D printing technology. *Chin J Med Phys*. 2016;33(9):6. doi:10.3969/j.issn.1005-202X.2016.09.011

39. Yusuff H, Zorn PE, Giraudeau C, *et al*. Development of a cost-effective 3D-printed MRI phantom to enhance teaching of system performance and image quality concepts. *Magn Reson Mater Phys Biol Med*. 2025;38(3):561-574. doi:10.1007/s10334-024-01217-z

40. Hindi OA, Pinarbasi B, Bakici M, *et al*. In situ bioprinting enhances bone regeneration in a live animal model of craniofacial defects. *ACS Biomater Sci & Eng*. 2025;11(12):5027-5037. doi:10.1021/acsbiomaterials.5c00780

41. Lee D, Ruf M, Karadimitriou N, *et al*. Development of stochastically reconstructed 3D porous media micromodels using additive manufacturing: numerical and experimental validation. *Sci Rep*. 2024;14(1):9375. doi:10.1038/s41598-024-60075-w

42. Zhang Z, Chen L, Sheng W, *et al*. Application of artificial intelligence in the diagnosis and treatment of lumbar disc herniation: evolution towards standardization, efficiency, and precision of diagnosis and treatment methods. *Chin J Tissue Eng Res*. 2025;29(29):6269-6276. doi:10.12307/2025.759

43. Wang L, Wang H, Jiang Y, *et al*. The efficacy and dosimetry analysis of CT-guided ^{125}I seed implantation assisted with 3D-printing non-co-planar template in locally recurrent rectal cancer. *Radiat Oncol*. 2020;15(1):179-183. doi:10.1186/s13014-020-01607-2

44. Gomez-Feria J, Narros J L, Go´ mez Ciriza G, *et al*. 3D printing of diffuse low-grade gliomas involving eloquent cortical areas and subcortical functional pathways: technical note. *World Neurosurg*. 2021;147:164-171. doi:10.1016/j.wneu.2020.12.082

45. Mangano FG, Yang KR, Lerner H, Admakin O, Mangano C. Artificial intelligence and mixed reality for dental implant planning: a technical note. *Clin Implant Dent Relat Res*. 2024;26(5):942-953. doi:10.1111/cid.13357

46. Winkel DJ, Mujagic E, Staub D, Harder D, Bremerich J, Obmann MM. Multimodal imaging and 3D printing of a thoracoabdominal aortic aneurysm eroding the spine. *Radiol Case Rep*. 2023;18(2):657-660. doi:10.1016/j.radcr.2022.11.020.

47. Minkenberg JG, Bender L, Franz C, *et al*. Accurate full-scale patient-specific Circle of Willis models including aneurysms: a novel manufacturing approach. *PLoS One*. 2025;20(7):e0328300. doi:10.1371/journal.pone.0328300

48. Holmes T W, Yin Z, Bujila R, *et al*. Ultrahigh-resolution K-edge imaging of coronary arteries with prototype deep-silicon photon-counting CT: initial results in phantoms. *Radiology*. 2024;311(3):e231598. doi:10.1148/radiol.231598.

49. Sato K, Yamashiro A, Koyama T. Material investigation for the development of non-rigid phantoms for CT-MRI image registration. *Nihon Hoshasen Gijutsu Gakkai Zasshi*. 2022;78(6):615-624. doi:10.6009/jjrt.2022-1241

50. Wang X, Zhao F, Zhen P. Physicochemical properties of 3D printed bioactive glass/hydroxyapatite bone repair materials. *J Ningxia Med Univ*. 2022;44(5):511-516. doi:10.16050/j.cnki.issn1674-6309.2022.05.013

51. Lichtenstein J, Heinzel S, Kurz B, *et al*. Are we ready for virtual planning and 3D-printed titanium plates in zygomatic fractures? A feasibility study based on 16 post-mortem fractures. *J Craniomaxillofac Surg*. 2025;53(3):325-331. doi:10.1016/j.jcms.2024.11.004

52. Jin Z, Zhang Z, Shao X, Gu GX. Monitoring anomalies in 3D bioprinting with deep neural networks. *ACS Biomater Sci Eng*. 2023;9(7):3945-3952. doi:10.1021/acsbiomaterials.0c01761

53. Zang XL, Sun J, Li YL, *et al*. 3D-bioprinting manufacturing polylactic-co-glycolic acid/nano-hydroxyapatite scaffold/bone morphogenetic protein-2 sustained release composite. *Chin J Tissue Eng Res*. 2016;20(16):2405-2411. doi:10.3969/j.issn.2095-4344.2016.16.017

54. Wu BY, Ye K, Chen JH, *et al*. Biocompatibility of 3D printed polyetheretherketone/hydroxyapatite composites. *Chin J Tissue Eng Res*. 2023;27(12):1932-1937. doi:10.12307/2023.079

55. Li P, Cheng W, Wang JQ, *et al*. Osteogenesis effect of bone marrow mesenchymal stem cells combined with bionic bone scaffold. *Henan Med Res*. 2022;31(7):1153-1158. doi:10.3969/j.issn.1004-437X.2022.07.001

56. Hu CR, Qiu B, Zhou ZX, Yang Y, Li J. In vitro biocompatibility of 3D printed polycaprolactone/nano-hydroxyapatite composite scaffold with bone marrow mesenchymal stem cells. *Chin J Tissue Eng Res*. 2020;24(4):589-595. doi:10.3969/j.issn.2095-4344.1880

57. Liu D, Qin H, Wang YX, *et al*. 3D-printed hydroxyapatite/polylactic acid network composites for skull defects. *Chin J Tissue Eng Res*. 2019;23(6):833-837. doi:10.3969/j.issn.2095-4344.0676

58. Silva G, Ashford R. Using artificial intelligence to predict outcomes of operatively managed neck of femur fractures. *Br J Hosp Med*. 2024;85(6):1-12. doi:10.12968/hmed.2024.0034

59. Fogarasi M, Coburn J C, Ripley B. Algorithms used in medical image segmentation for 3D printing and how to understand and quantify their performance. *3D Print Med*. 2022;8(1):18. doi:10.1186/s41205-022-00145-9

60. Yang B, Gong K, Liu H, Li Q, Zhu W. Anatomically guided pet image reconstruction using conditional weakly-supervised multi-task learning integrating self-attention. *IEEE Trans Med Imaging*. 2024;43(6):2098-2112. doi:10.1109/TMI.2024.3356189